JACS
JOURNAL OF THE AMERICAN CHEMICAL SOCIETY
Communication
pubs.acs.org/JACS

In Situ Synthesis of Highly Dispersed and Ultrafine Metal Nanoparticles from Chalcogels

Jian Liu,[†,‡] Kai He,[§] Weiqiang Wu,[†] Tze-Bin Song,[†] and Mercouri G. Kanatzidis*[,†,‡,§]

[†]Department of Chemistry, [‡]Argonne-Northwestern Solar Energy Research Center, [§]Department of Materials Science and Engineering, Northwestern University, Evanston, Illinois 60208, United States

Supporting Information

ABSTRACT: We report a unique reaction type for facile synthesis of ultrafine and well-dispersed Pt nanoparticles supported on chalcogel surfaces. The nanoparticles are obtained by in situ Pt^{2+} reduction of a chalcogel network formed by the metathesis reaction between K_2PtCl_4 and Na_4SnS_4. The rapid catalytic ability of the chalcogel-supported Pt nanoparticles is demonstrated in a recyclable manner by using 4-nitrophenol reduction as a probe reaction.

Ultrafine metal nanoparticles (NPs) have unique physical and chemical properties and are important in optoelectronics, plasmonics and catalysis.[1−3] Especially, ultrafine noble metal NPs (Pd, Pt, Au) with large surface area and number of edge and corner atoms are greatly beneficial to catalysis.[4,5] The behavior and stability of noble metal NP catalysts, however, can be greatly hampered due to agglomeration. Supporting substrates are usually required to disperse the NPs, which keep them from aggregation, secure easy separation after the reaction and deliver favorable catalytic behavior and stability.[6−8] Mesoporous materials (such as silica, carbon and titania) with interconnected mesochannels as well as metal organic framework are appealing as supporting substrates because of the ease of fabrication, higher surface areas, and stability.[9−23] Dispersing noble metal NPs onto the supports has been achieved by microwave irradiation, impregnation, deposition-precipitation, photodeposition, chemical vapor deposition, atomic layer deposition, etc.[4,7,20] The nanointerface between noble metal NPs and the underlying substrates largely determines the catalytic behavior and stability.[6,24,25] For example, if the underlying substrates participate in catalytic reactions, the weak interactions between the substrates and noble metal NPs can limit catalytic activity.[24] Therefore, developing a synthesis strategy that can simultaneously address both the dispersion and nanointerface issues is appealing.

The in situ formation of the NPs on the supported substrates addressing aggregation and interface engineering issues is highly desirable for diverse applications including catalysis.[24,26,27] For example, noble metal precursors incorporated in polymers can be reduced to form immobilized NPs on the surface of nanodiamonds, and have shown good stability toward catalyzing $NaBH_4$ reduction of the 4-nitrophenol.[28] Solution-phase epitaxial growth of noble metal nanostructures on dispersible MoS_2 nanosheets was also reported.[29] In these examples, the in situ formation of the supported NPs is mostly based on the separate metal sources. In the vast amounts of reported examples, NPs are mostly supported on metal oxide or carbon surfaces. Here we describe a reaction type that can yield NPs supported on sulfidic and more generally chalcogenide surfaces and the NPs derive from the substrate itself.

Previously, we reported a generalized strategy to synthesize highly porous semiconducting aerogels (chalcogels) from chalcogenide-based clusters ($[M_nQ_{2n+2}]^{4-}$, M = Ge, Sn; Q = S, Se, n = 1, 2, 4) and the linking metal ions (such as Pt^{2+}, Sn^{2+}, Sb^{3+}). We have shown diverse applications for these materials including ion adsorption, gas separation, catalysis, electrocatalysis and photocatalysis.[30−39] Here we show that using a suitable reductant, the Pt metal centers in a Pt−Sn−S chalcogel structure can be reduced while the remaining Pt−Sn−S chalcogel skeleton acts as the supporting substrate. Specifically, we describe a unique method for the in situ generation of supported Pt NPs involving the use of Pt^{2+} containing chalcogel (abbreviated as Pt-$SnS_{pristine}$) as the precursor. Well-dispersed and ultrafine Pt NPs supported on the chalcogel skeleton are obtained after reduction with $NaBH_4$. The material obtained by the in situ formed NPs on chalcogel catalyzes the rapid reduction of 4-nitrophenol to 4-aminophenol. The quick and complete conversion suggests the formed NPs as an excellent hydrogenation catalyst and good recyclability proved the stability of the system. The route could be applied to other noble metals, such as Pd, Au and Ag, and even for controllable synthesis of supported alloy NPs in the future.

The synthesis of Pt containing chalcogel (abbreviated as the Pt-$SnS_{pristine}$) is from the metathesis reaction between K_2PtCl_4 and $Na_4SnS_4{\cdot}14H_2O$ in deionized water. Upon mixing of the precursor solutions, the purple solution starts to turn yellowish accompanying the gelation process, which lasts 5−6 h (see Figure S1 of Supporting Information, abbreviated as SI). After gelation, the as-obtained chalcogel is washed extensively with water to remove the unnecessary byproducts of NaCl and KCl. A xerogel is obtained after drying of the cleaned chalcogel in the nitrogen glovebox and supercritical drying with liquid CO_2 results in the aerogel. This material contains Pt^{2+} ions as linking atoms for the $[SnS_4]^{4-}$ but contains no Pt NPs.

The transmission electron microscopy (TEM) image in Figure 1a and high-resolution TEM (HRTEM) image of Pt-$SnS_{pristine}$ chalcogel in Figure 1b suggest that the chalcogel skeleton is homogeneous. No Pt NPs could be observed. The selected area electron diffraction (SAED) shown in the inset of

Received: December 26, 2016
Published: February 13, 2017

DOI: 10.1021/jacs.6b13279
J. Am. Chem. Soc. 2017, 139, 2900−2903

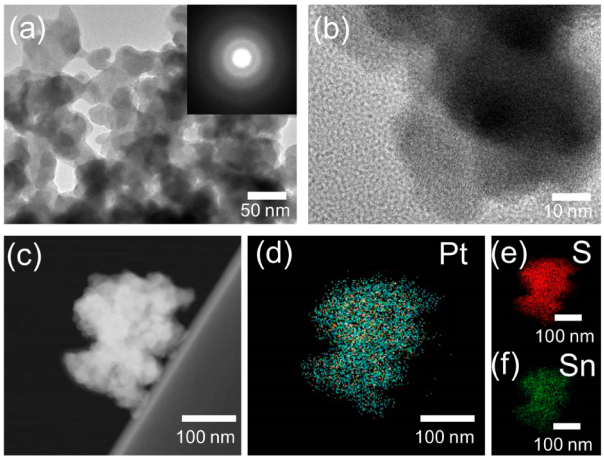

Figure 1. (a) TEM image of the Pt-$SnS_{pristine}$ chalcogel with inset showing the diffuse e-beam scattering arising from the amorphous nature of the gel. (b) HRTEM image of the Pt-$SnS_{pristine}$ chalcogel indicating the absence of Pt NPs. (c) HAADF-STEM image of the Pt-$SnS_{pristine}$ gel. (d–f) EDS mapping of composition elements, Pt, S and Sn, in the Pt-$SnS_{pristine}$ gel, respectively.

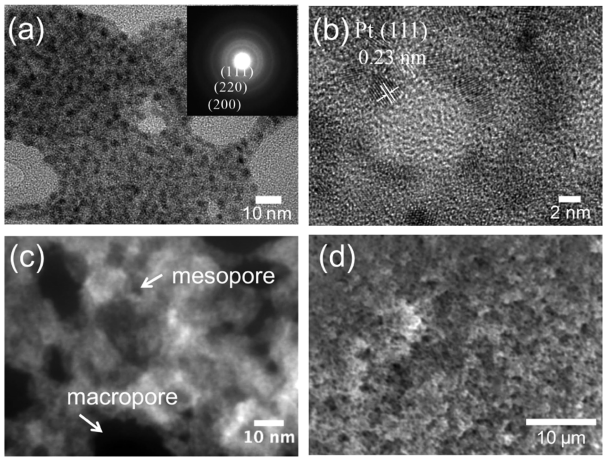

Figure 2. (a) TEM image of the Pt-$SnS_{reduced}$ xerogel shows the presence of the well-dispersed Pt NPs in the chalcogel skeleton and inset shows the polycrystalline nature of the gel. (b) HRTEM image of the Pt-$SnS_{reduced}$ xerogel. (c) HAADF-STEM image of the Pt-$SnS_{reduced}$ gel. (d) SEM image of the Pt-$SnS_{reduced}$ xerogel.

Figure 1a demonstrates the amorphous nature of the chalcogel, although both precursors (see Figure S2 of SI) give strong diffraction peaks from X-ray diffraction (XRD) patterns (as illustrated in Figure S3 of SI). The spatial confinement of Pt^{2+} in the chalcogel network was verified by the high-angle annular dark-field scanning transmission electron microscopy (HAADF-STEM) and the energy-dispersive X-ray spectroscopy (EDS). The HAASD-STEM imaging in Figure 1c shows uniform Z-contrast (proportional to atomic number), indicating the homogeneous distribution of Pt^{2+} with respect to all composition elements of the gel. The corresponding EDS maps in Figure 1d,e,f demonstrate that the constituent elements (Pt, S and Sn) are distributed uniformly in the chalcogel network (see also Figure S4 of SI). Area-averaged EDS compositions of the Pt-$SnS_{pristine}$ xerogel indicate an empirical formula close to "$NaKPtSnS_4$" (Figure S5 and S6 of SI). The Pt–Sn–S network is negatively charged, with the K^+ and Na^+ cations balancing the charge. The weight ratio of Pt^{2+} in the pristine gel is about 50% from the EDS analysis (Figure S6c of SI).

To precipitate in situ the Pt NPs out of the chalcogel, the Pt-$SnS_{pristine}$ chalcogel is mixed with a $NaBH_4$ aqueous solution. After mixing, hydrogen bubbles are observed due to the spontaneous hydrolysis of $NaBH_4$, and the monolith chalcogel breaks into small pieces with the color turning from light yellow to brownish gradually. The Pt^{2+} is reduced by the $NaBH_4$ or the nascent hydrogen and nucleated rapidly on the gel network to grow into clusters and further into NPs. The accompanying dark brown color arising from the plasmonic absorbance indicates the formation of the Pt NPs.

The TEM image in Figure 2a indicates the well-dispersed and supported Pt NPs in the chalcogel network (abbreviated as Pt-$SnS_{reduced}$). The size of the ultrafine Pt NPs is around 2 nm but the range is from 1.5 to 4.2 nm (after statistics of 50 NPs). The in situ reduction of Pt^{2+} from the chalcogel network leads to the supported NPs directly formed on chalcogel skeleton. The corresponding SAED pattern in the inset of Figure 2a indicates the polycrystalline nature of the Pt NPs and the electron diffraction pattern of Pt NPs indicates the characteristic Bragg peaks at (111), (220) and (200). The HRTEM image in Figure 2b shows the lattice fringe spacing of 0.232 nm corresponds to the (111) plane of face-centered cubic Pt crystal. Comparing with the amorphous Pt-$SnS_{pristine}$, the reduced counterpart appears to possess more porosity from the darker area observed by HAADF-STEM, which is due to the formation of Pt NPs from the network, see Figure 2c. The SEM image in Figure 2d depicts the porous and spongy nature of the reduced chalcogel which does not appear to have been morphologically altered after reduction.

The N_2 adsorption–desorption isotherms are shown in Figure 3a. The Brunauer–Emmett–Teller (BET) surface areas

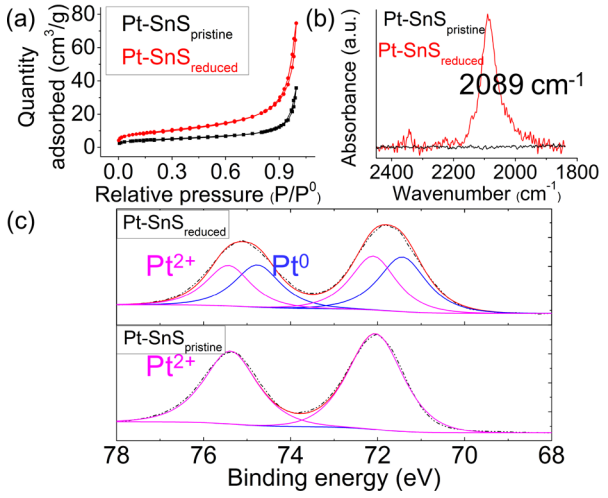

Figure 3. (a) N_2 adsorption and desorption isotherms of the Pt-$SnS_{pristine}$ and Pt-$SnS_{reduced}$ aerogels at 77 K. (b) DRIFTS investigation of CO adsorption on the reduced and Pt-$SnS_{pristine}$ xerogels, respectively. (c) Pt 4f XPS spectra of the pristine and Pt-$SnS_{reduced}$ xerogels, respectively.

of the pristine and Pt-$SnS_{reduced}$ aerogel were 30 and 52 m^2/g, respectively. The enhanced surface area after $NaBH_4$ reduction is probably due to the breakage of the chalcogel to expose more open sites, which is beneficial for potential catalysis applications (see pore size distributions in Figure S7 of SI). The XRD characterization of the Pt-$SnS_{reduced}$ xerogel suggests the amorphous nature of the gel like the pristine xerogel (Figure

DOI: 10.1021/jacs.6b13279
J. Am. Chem. Soc. 2017, 139, 2900–2903

S8 of SI). The lack of diffraction peaks of the metallic Pt NPs could probably be attributed to the small grain size (~2 nm) and high dispersion of Pt NPs in the chalcogel network. Infrared spectroscopy of CO adsorption on supported noble metal catalysts is widely used to determine the atomic and electronic structures of the binding sites.[40,41] Herein, the diffuse reflectance infrared Fourier transform spectroscopy (DRIFTS) was adopted to investigate the CO adsorption on the Pt-$SnS_{reduced}$ sample. As shown in Figure 3b, the newly formed peak at 2089 cm^{-1} is assigned to the CO adsorption on the Pt NPs, in agreement with literature reports.[41] For reference, a CO adsorption peak does not appear when using the pristine Pt-SnS gel or K_2PtCl_4 under our experimental conditions (Figure S9 of SI), indicating that Pt NPs are the binding species of CO.

From the X-ray photoelectron spectroscopy (XPS) results in bottom part of Figure 3c, the platinum(II) is exclusively present in the Pt-$SnS_{pristine}$ gel. However, the slight decrease of the binding energy of Pt $4f_{7/2}$ from 72.8 eV in K_2PtCl_4 (Figure S10a of SI) to 72.1 eV demonstrates the slight decrease of oxidation state of Pt^{2+} after metathesis reaction due to the replacement of the electronegative Cl^- by less electronegative terminal sulfur atoms of $[SnS_4]^{4-}$.[30] After $NaBH_4$ reduction, the existence of Pt^0 is clearly observed along with Pt^{2+} in the structure of the Pt-SnS gel (upper part of Figure 3c). The Pt^0:Pt^{2+} ratio could be further adjusted by the $NaBH_4$ amount. Some Sn^{4+} was reduced to Sn^{2+} in the process. The XPS spectra of Sn 3d is shown in Figure S11 of SI. By controlling the amount of $NaBH_4$, samples containing various amounts ranging from traces of Pt^0 to complete Pt^0 could be obtained (See Figure S10b,c of SI). The partially reduced gel with comparable amount of Pt^0 and Pt^{2+} (upper part of Figure 3c) was employed in the characterization and catalytic testing.

The catalytic behavior of noble metal NPs is typically evaluated by the reduction of 4-nitrophenol to 4-aminophenol using $NaBH_4$.[42,43] The reduction reaction does not occur without the Pt-$SnS_{pristine}$ chalcogel catalyst, as shown by the constant absorption peak at 400 nm in the UV−vis spectrum (Figure S12a of SI). The Na_4SnS_4 itself does not show any activity toward 4-nitrophenol reduction. K_2PtCl_4 could be directly reduced by $NaBH_4$ to obtain Pt NPs, which could further catalyze the reduction of 4-nitrophenol. However, aggregation of in situ formed Pt particles was severe, which underscores the importance of the supporting substrate (as shown in Figure S13 of SI). As shown in Figure 4a, full conversion of 4-nitrophenol to 4-aminophenol is accomplished in 10 min with the diminish of the peak at 400 nm in the UV−vis spectra. The inset of Figure 4a shows the discoloration of the solution after full conversion. We further investigated the recyclability of the Pt-$SnS_{reduced}$ catalyst in the 4-nitrophenol reduction experiment. After centrifugation and washing with deionized water, the recovered Pt-$SnS_{reduced}$ was reused to perform additional catalytic experiments. Conversion rates above 90% could still be achieved after 5 cycles (see Figure S12b of SI). The TEM of the recycled Pt-SnS materials was similar to the original materials demonstrating the robustness of the Pt NPs (see Figure S14 of SI). Because the presence of $NaBH_4$ for catalytic conversion of 4-nitrophenol would cause the breakage of the chalcogel network and reduction of the Pt^{2+} to Pt NPs, we also perform the 4-nitrophenol reduction with the Pt-$SnS_{pristine}$ chalcogel. As shown by the green column in Figure 4b, a comparable conversion was achieved with the Pt-$SnS_{pristine}$, indicating that the tandem formation of Pt NPs and subsequent catalysis occur with $NaBH_4$ participating in both reactions. The Pt NPs after this tandem reaction were observed to possess slightly larger size and aggregation behavior (Figure S15 of SI).

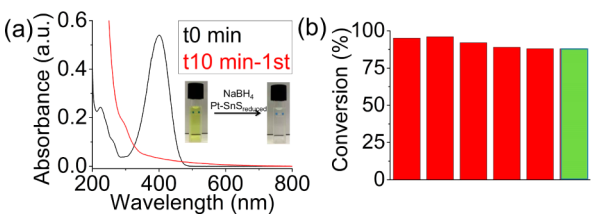

Figure 4. (a) UV−vis spectra and typical optical image (inset) before and after catalysis of the Pt-$SnS_{reduced}$, respectively. (b) Stability investigation in 5 consecutive catalysis experiments; the last histogram column shows the behavior of the Pt-$SnS_{pristine}$ chalcogel (without reduction in advance) for reduction of 4-nitrophenol in the presence of $NaBH_4$.

In conclusion, well-dispersed and supported ultrafine Pt NPs are obtained by the in situ reduction of Pt^{2+} from the Pt−Sn−S chalcogel network using $NaBH_4$. The good dispersion of Pt NPs in the chalcogel surface is derived from the homogeneous nature of the chalcogel. The catalytic behavior of the chalcogel-supported NPs has been demonstrated by the reduction of 4-nitrophenol to 4-aminophenol in a quick and recyclable manner. Further diversifying the metal species (Pd, Au, Ag) and chalcogenide clusters (polysulfide, $Na_4Sn_2S_6$, Na_4SbS_3, Na_4SbS_4, etc.) will provide more opportunities to modulate the size, distribution and compositions of noble metal NPs on support. We postulate that chalcogel-derived in situ growth of metal NPs supported on chalcogenide surfaces is a promising path for functional composite nanomaterials.

■ ASSOCIATED CONTENT

Supporting Information

The Supporting Information is available free of charge on the ACS Publications website at DOI: 10.1021/jacs.6b13279.

Experimental section, SEM, TEM, XPS, DRIFTS characterizations (PDF)

■ AUTHOR INFORMATION

Corresponding Author

*m-Kanatzidis@northwestern.edu

ORCID

Jian Liu: 0000-0002-9684-339X

Mercouri G. Kanatzidis: 0000-0003-2037-4168

Notes

The authors declare no competing financial interest.

■ ACKNOWLEDGMENTS

This work was supported as part of the ANSER Center, an Energy Frontier Research Center funded by the U.S. Department of Energy, Office of Science, Office of Basic Energy Sciences, under award no. DE-SC0001059.

■ REFERENCES

(1) Sau, T. K.; Rogach, A. L.; Jäckel, F.; Klar, T. A.; Feldmann, J. *Adv. Mater.* **2010**, *22*, 1805.
(2) Liz-Marzán, L. M. *Langmuir* **2006**, *22*, 32.
(3) Eustis, S.; El-Sayed, M. A. *Chem. Soc. Rev.* **2006**, *35*, 209.
(4) Li, X.-H.; Wang, X.; Antonietti, M. *Chem. Sci.* **2012**, *3*, 2170.

DOI: 10.1021/jacs.6b13279
J. Am. Chem. Soc. 2017, 139, 2900−2903

(5) Li, C.; Jiang, B.; Miyamoto, N.; Kim, J. H.; Malgras, V.; Yamauchi, Y. *J. Am. Chem. Soc.* **2015**, *137*, 11558.
(6) Li, X.-H.; Antonietti, M. *Chem. Soc. Rev.* **2013**, *42*, 6593.
(7) White, R. J.; Luque, R.; Budarin, V. L.; Clark, J. H.; Macquarrie, D. J. *Chem. Soc. Rev.* **2009**, *38*, 481.
(8) Dhakshinamoorthy, A.; Garcia, H. *Chem. Soc. Rev.* **2012**, *41*, 5262.
(9) Liu, J.; Li, M.; Zhou, J.; Ye, C.; Wang, J.; Jiang, L.; Song, Y. *Appl. Phys. Lett.* **2011**, *98*, 023110.
(10) Wang, S.; Zhao, Q.; Wei, H.; Wang, J.-Q.; Cho, M.; Cho, H. S.; Terasaki, O.; Wan, Y. *J. Am. Chem. Soc.* **2013**, *135*, 11849.
(11) Datta, K.; Reddy, B.; Ariga, K.; Vinu, A. *Angew. Chem., Int. Ed.* **2010**, *49*, 5961.
(12) Li, Z.; Liu, J.; Huang, Z.; Yang, Y.; Xia, C.; Li, F. *ACS Catal.* **2013**, *3*, 839.
(13) Zhu, F.-X.; Wang, W.; Li, H.-X. *J. Am. Chem. Soc.* **2011**, *133*, 11632.
(14) Shang, L.; Bian, T.; Zhang, B.; Zhang, D.; Wu, L. Z.; Tung, C. H.; Yin, Y.; Zhang, T. *Angew. Chem., Int. Ed.* **2014**, *53*, 250.
(15) Yang, C.-H.; Wang, W.-T.; Grumezescu, A. M.; Huang, K.-S.; Lin, Y.-S. *Nanoscale Res. Lett.* **2014**, *9*, 277.
(16) Parlett, C. M.; Isaacs, M. A.; Beaumont, S. K.; Bingham, L. M.; Hondow, N. S.; Wilson, K.; Lee, A. F. *Nat. Mater.* **2016**, *15*, 178.
(17) Xie, Y.; Ding, K.; Liu, Z.; Tao, R.; Sun, Z.; Zhang, H.; An, G. *J. Am. Chem. Soc.* **2009**, *131*, 6648.
(18) Zheng, Z.; Huang, B.; Qin, X.; Zhang, X.; Dai, Y.; Whangbo, M.-H. *J. Mater. Chem.* **2011**, *21*, 9079.
(19) Yang, H.; Bradley, S. J.; Chan, A.; Waterhouse, G. I.; Nann, T.; Kruger, P. E.; Telfer, S. G. *J. Am. Chem. Soc.* **2016**, *138*, 11872.
(20) Lu, G.; Li, S.; Guo, Z.; Farha, O. K.; Hauser, B. G.; Qi, X.; Wang, Y.; Wang, X.; Han, S.; Liu, X.; DuChene, J. S.; Zhang, H.; Zhang, Q.; Chen, X.; Ma, J.; Loo, S. C. J.; Wei, W. D.; Yang, Y.; Hupp, J. T.; Huo, F. *Nat. Chem.* **2012**, *4*, 310.
(21) Dong, F.; Guo, W.; Park, S.-K.; Ha, C.-S. *Chem. Commun.* **2012**, *48*, 1108.
(22) Vamvasakis, I.; Liu, B.; Armatas, G. S. *Adv. Funct. Mater.* **2016**, *26*, 8062.
(23) Hitihami-Mudiyanselage, A.; Senevirathne, K.; Brock, S. L. *Chem. Mater.* **2014**, *26*, 6251.
(24) Zhang, Z.-c.; Xu, B.; Wang, X. *Chem. Soc. Rev.* **2014**, *43*, 7870.
(25) Mohanan, J. L.; Arachchige, I. U.; Brock, S. L. *Science* **2005**, *307*, 397.
(26) Zhong, L.-S.; Hu, J.-S.; Cui, Z.-M.; Wan, L.-J.; Song, W.-G. *Chem. Mater.* **2007**, *19*, 4557.
(27) Zhou, X.; Huang, X.; Qi, X.; Wu, S.; Xue, C.; Boey, F. Y.; Yan, Q.; Chen, P.; Zhang, H. *J. Phys. Chem. C* **2009**, *113*, 10842.
(28) Quast, A. D.; Bornstein, M.; Greydanus, B. J.; Zharov, I.; Shumaker-Parry, J. S. *ACS Catal.* **2016**, *6*, 4729.
(29) Huang, X.; Zeng, Z.; Bao, S.; Wang, M.; Qi, X.; Fan, Z.; Zhang, H. *Nat. Commun.* **2013**, *4*, 1444.
(30) Bag, S.; Trikalitis, P. N.; Chupas, P. J.; Armatas, G. S.; Kanatzidis, M. G. *Science* **2007**, *317*, 490.
(31) Bag, S.; Arachchige, I. U.; Kanatzidis, M. G. *J. Mater. Chem.* **2008**, *18*, 3628.
(32) (a) Liu, J.; Kelley, M. S.; Wu, W.; Banerjee, A.; Douvalis, A. P.; Wu, J.; Zhang, Y.; Schatz, G. C.; Kanatzidis, M. G. *Proc. Natl. Acad. Sci. U. S. A.* **2016**, *113*, 5530. (b) Banerjee, A.; Yuhas, B. D.; Margulies, E. A.; Zhang, Y.; Shim, Y.; Wasielewski, M. R.; Kanatzidis, M. G. *J. Am. Chem. Soc.* **2015**, *137*, 2030.
(33) Subrahmanyam, K. S.; Malliakas, C. D.; Sarma, D.; Armatas, G. S.; Wu, J.; Kanatzidis, M. G. *J. Am. Chem. Soc.* **2015**, *137*, 13943.
(34) Subrahmanyam, K. S.; Sarma, D.; Malliakas, C. D.; Polychronopoulou, K.; Riley, B. J.; Pierce, D. A.; Chun, J.; Kanatzidis, M. G. *Chem. Mater.* **2015**, *27*, 2619.
(35) Shafaei-Fallah, M.; Rothenberger, A.; Katsoulidis, A. P.; He, J.; Malliakas, C. D.; Kanatzidis, M. G. *Adv. Mater.* **2011**, *23*, 4857.
(36) Shafaei-Fallah, M.; He, J.; Rothenberger, A.; Kanatzidis, M. G. *J. Am. Chem. Soc.* **2011**, *133*, 1200.
(37) Oh, Y.; Bag, S.; Malliakas, C. D.; Kanatzidis, M. G. *Chem. Mater.* **2011**, *23*, 2447.
(38) Katsoulidis, A. P.; He, J.; Kanatzidis, M. G. *Chem. Mater.* **2012**, *24*, 1937.
(39) (a) Staszak-Jirkovský, J.; Malliakas, C. D.; Lopes, P. P.; Danilovic, N.; Kota, S. S.; Chang, K.-C.; Genorio, B.; Strmcnik, D.; Stamenkovic, V. R.; Kanatzidis, M. G.; Markovic, N. M. *Nat. Mater.* **2016**, *15*, 197. (b) Yuhas, B. D.; Smeigh, A. L.; Samuel, A. P. S.; Shim, Y.; Bag, S.; Douvalis, A. P.; Wasielewski, M.; Kanatzidis, M. G. *J. Am. Chem. Soc.* **2011**, *133*, 7252. (c) Yuhas, B. D.; Prasittichai, C.; Hupp, J. T.; Kanatzidis, M. G. *J. Am. Chem. Soc.* **2011**, *133*, 15854. (d) Yuhas, B. D.; Smeigh, A. L.; Douvalis, A. P.; Wasielewski, M. R.; Kanatzidis, M. G. *J. Am. Chem. Soc.* **2012**, *134*, 10353. (e) Shim, Y.; Yuhas, B. D.; Dyar, S. M.; Smeigh, A. L.; Douvalis, A. P.; Wasielewski, M. R.; Kanatzidis, M. G. *J. Am. Chem. Soc.* **2013**, *135*, 2330. (f) Shim, Y.; Young, R. M.; Douvalis, A. P.; Dyar, S. M.; Yuhas, B. D.; Bakas, T.; Wasielewski, M. R.; Kanatzidis, M. G. *J. Am. Chem. Soc.* **2014**, *136*, 13371.
(40) Zaera, F. *Chem. Soc. Rev.* **2014**, *43*, 7624.
(41) Ding, K.; Gulec, A.; Johnson, A. M.; Schweitzer, N. M.; Stucky, G. D.; Marks, L. D.; Stair, P. C. *Science* **2015**, *350*, 189.
(42) Deng, Y.; Cai, Y.; Sun, Z.; Liu, J.; Liu, C.; Wei, J.; Li, W.; Liu, C.; Wang, Y.; Zhao, D. *J. Am. Chem. Soc.* **2010**, *132*, 8466.
(43) Liu, R.; Mahurin, S. M.; Li, C.; Unocic, R. R.; Idrobo, J. C.; Gao, H.; Pennycook, S. J.; Dai, S. *Angew. Chem., Int. Ed.* **2011**, *50*, 6799.

DOI: 10.1021/jacs.6b13279
J. Am. Chem. Soc. 2017, 139, 2900−2903